RSC Advances

ROYAL SOCIETY OF CHEMISTRY

www.rsc.org/advances

Title:

Pyoverdin mediated sunlight induced green synthesis of silver nanoparticles

Authors:

Prashant R. Dane, Shraddha P. Pawar, Raksha A. Kankariya and Bhushan L. Chaudhari*

Affiliations:

Department of Microbiology, School of Life Sciences, North Maharashtra University, P. Box 80, Jalgaon - 425001 Maharashtra, India

***Corresponding author:**

Department of Microbiology, School of Life Sciences,

North Maharashtra University, Jalgaon, Maharashtra, India.

<blchaudhari@hotmail.com>, <blchaudhari@nmu.ac.in>

Abstract:

The objective of this work was to check the ability of a siderophore; pyoverdin; a natural iron chelating compound of a bacterial origin to produce silver nanoparticles (AgNps) under sunlight. Among the 26 strains of siderophore producing fluorescent Pseudomonads, strain SBC-I was found to be latent applicant based on its percent decoloration of chrome azurol sulfonate reagent. The 16s rRNA gene sequence revealed the strain SBC-I to be *Pseudomonas aeruginosa* owing to 99% similarity with previously reported culture. The silver ions were examined for its coordination with the purified pyoverdin using UV-Vis spectrophotometric titrations. The AgNps were found crystallized in the face centered cubic with an average particle size of 6-12 nm. The predicted mechanism of AgNps synthesis involved photoreduction of metal ions by means of ligand-to-metal charge transfer. The synthesis of AgNps was confirmed by transmission electron microscopy, X-ray diffraction, attenuated total reflection-Fourier transform infrared spectroscopy and UV-Vis spectrophotometry. Synthesized AgNps showed antibacterial activity against *Salmonella typhi*, *Escherichia coli*, *Bacillus spizizenii* and *Staphylococcus aureus*.

Keywords: *Pseudomonas aeruginosa*; Siderophore; Pyoverdin; Silver nanoparticles; Antibacterial potential

1. Introduction:

Siderophores are the low molecular weight ligands produced in response to non availability of soluble iron in the environment [1]. The stability constants (β) of various siderophore molecules for their iron complexation range from 10^{10} to 10^{49} [2, 3]. Fluorescent pseudomonads present in the soil and water are screened on the basis of their abilities to synthesize siderophore, pyoverdin which is a water-soluble yellow-green pigment produced under iron-deficient conditions [4]. A culture *Pseudomonas aeruginosa* is known to produce siderophores mainly pyoverdin and pyochelin that play an important role in bacterial virulence [5]. Apart from iron chelation, pyoverdin is also reported to chelate Ag^{+}, Al^{3+}, Cd^{2+}, Co^{2+}, Cr^{2+}, Cu^{2+}, Eu^{3+}, Ga^{3+}, Hg^{2+}, Mn^{2+}, Ni^{2+}, Pb^{2+}, Sn^{2+}, Tb^{3+}, Tl^{+} and Zn^{2+} [6]. The metal-microbe interactions or more precisely, metal-chelator interactions play important roles in bioremediation, biomineralization and bioleaching.

The synthesis of silver and gold nanoparticles using various biological materials has remained the thrust area. A bacterium *Pseudomonas aeruginosa* has been reported for the synthesis of gold [7] and silver nanoparticles with the projected involvement of metabolites like rhamnolipids and an antibiotic phenazine-1-carboxylic acid [8, 9]. A copper chelator; methanobactin produced by methanotrophs was observed to synthesize gold nanoparticles [10]. However, the ability of a siderophore pyoverdin (PVD); a naturally occurring strong iron chelating ligand to produce silver nanoparticles remains obscure. In this study, we report the PVD mediated sunlight-induced rapid synthesis of silver nanoparticles (AgNps) using $AgNO_3$ as a starting material. The PVD was biologically synthesized from *P. aeruginosa*, purified and partially characterized. Its UV-Vis spectroscopic interaction with silver ions was studied and a possible mechanism of AgNps synthesis is proposed here. Synthesized AgNps were characterized and its antibacterial activity was also checked against human pathogens.

2. Materials and methods:

2.1 Chemicals, glassware and Pathogenic bacteria:

All the chemicals and media were purchased from Hi-Media (Mumbai). All of the glassware were immersed in 6 M HCl for overnight period, further washed with Milli Q deionized water and this practice was observed throughout the experiment. Chrome azurol sulfonate (CAS) assay ingredients such as Chrome Azurol S reagent, hexadecyltrimethylammonium bromide (HDTMA) were purchased from Sigma (Banglore) and piperazine from Hi-Media (Mumbai). Human bacterial pathogens, *viz. Bacillus spizizenii (*ATCC 6633)*, Staphylococcus aureus* (ATCC 6538)*, Escherichia coli* (ATCC 8739) and *Salmonella typhi* (NCIM 2501) were used and stored at 4 ^{0}C.

2.2 Isolation of fluorescent Pseudomonads:

Rhizosperhic soil samples of cotton were collected from fertile agricultural land nearby. The roots were washed with sterile saline and some of its parts were inoculated into King's B broth for the enrichment at 28 ^{0}C with shaking at 120 rpm for 48 h. Enriched sample was serially diluted and streaked on solid King's B medium and incubated at 28 ^{0}C. Colonies obtained were checked for green fluorescence under ultraviolet light (254-365 nm) using UV trans-illuminator and stored on the slants of the same medium in tubes.

2.3 Screening and identification of siderophore producing *Pseudomonas sp*.:

All the Pseudomonad isolates were screened for the siderophore production by Csaky and Arnow's assay for siderophore type using cell free supernatant [11, 12] upon growing in 50 ml of succinate medium (SCM), pigment production medium (PPM) and King's B medium (KBM) respectively in 250 ml culture flasks. The ability of these isolates to produce siderophores was confirmed by universal Chrom Azurol S assay for siderophores [13]. On the basis of highest percent decolorization [14], a culture SBC-I was selected and subjected for

molecular identification using by 16s rRNA gene sequencing and further studies (Applied BioSystems, USA).

2.4 Evolutionary relationship of a culture SBC-I:

The evolutionary history was inferred using the Neighbor-Joining method [15] of rRNA gene sequences. The optimal tree with the sum of branch length was 0.4121. The percentage of replicate trees in which the associated taxa clustered together in the bootstrap test (2000 replicates) was shown next to the branches [16]. The tree was drawn to scale, with branch lengths in the same units as the evolutionary distances were used to infer the phylogenetic tree. The evolutionary distances were computed using the Kimura 2-parameter method [17] and are in the units of the number of base substitutions per site. The analysis involved 14 nucleotide sequences of other known cultures. Codon positions included were 1st+2nd+3rd+Noncoding. All positions containing gaps and missing data were eliminated. There were a total of 721 positions in the final dataset. Evolutionary analyses were conducted in MEGA 6 programme [18].

2.5 Siderophore production, purification and characterization:

2.5.1 Fermentative Production:

Siderophore production by culture SBC-I was carried out in iron free SCM (g/l: KH_2PO_4, 6; K_2HPO_4, 3; $(NH_4)_2SO_4$, 1; $MgSO_4.7H_2O$, 0.2; Na-succinate, 4) and pH was adjusted to 7.0 by using 6 N NaOH solution prior to sterilization [19]. It was inoculated with 24 h freshly grown culture and incubated at 28 ^{0}C under aerobic condition with shaking at 120 rpm for 48 h.

2.5.2 Purification and Characterization of Siderophore:

Upon growth of culture SBC-I for 48 h, it was centrifuged at ~ 4000 g at 4^{0}C for 15 min to separate the biomass. The culture free supernatant acidified to pH 4.0 with 6M HCl was

loaded to Amberlite^{TM} XAD - 4 (Hi Media, Mumbai) resin column (18 x 300 mm) for adsorption and eluted with 100% methanol at a flow rate of 3 ml/min. The eluted fractions bearing CAS +ve test having identical UV absorption peaks at 230 nm and 400 nm were pooled together and dried under vacuum using rotary vacuum evaporator (R-124 BUCHI, Switzerland) at 45 - 50 ^{0}C. The dried powder was dissolved in pure water (Type I Mili-Q water (Milipore, USA) at 1:1 (w/v) and further loaded on pre-equilibrated affinity cum size exclusion column (Sephadex^{TM} LH 20, GE Healthcare, Sweden) which was eluted with 50% methanol. The eluted fractions were collected with flow rate of 1 ml/min and pooled together as mentioned in the previous step and dried under vaccum. Later, this vacuum dried sample was loaded on Biogel P – 2 gel filtration column (Bio-Rad, USA). Upon elution with phosphate buffer (0.1 M, pH 7.0), the CAS positive fractions were pooled, lyophilized and the powdered siderophore was characterized before interaction studies with silver [20].

2.5.3 HPLC:

The purified siderophore was subjected to HPLC (LC-8A, Shimadzu, Japan) using Eurospher C_{18} reverse phase column (100-5, 250 x 4.6 mm with pre-column) equipped with detector (190 – 600 nm) and methanol-water (70:30 v/v) as mobile phase at a flow rate of 0.5 ml/min (programmed for 15 min).

2.5.4 ATR-FTIR:

The purified siderophore was then subjected to structural characterization using Attenuated Total Reflection- FTIR spectrometer (88522 Spectrum Two TM, Perkin-Elmer, USA) in the range of 4000 – 400 cm^{-1} with 45 scans accumulation at a spectral resolution of 4 cm^{-1}.

2.6 Spectrophotometric titration of $AgNO_3$ with PVD:

All UV-visible spectra were determined using a quartz cuvette with a 1.0-cm path length and recorded using spectrophotometer (SL 244 Elico, India) at 25 ^{0}C. The titration of the Ag^{+} (1 X 10^{-3} M) against the isolated siderophore; PVD (1 X 10^{-5} M) was performed at pH 7.0 and monitored by UV–visible absorption spectroscopy at every 30 s up to 120 min.

2.7 PVD assisted green synthesis of AgNps:

The stoichiometric data of PVD and Ag^{+} generated upon the titration was used to determine their appropriate molar concentration based upon which equimolar concentration (1mM each) was used for the synthesis of AgNps. The said mixture was exposed to sunlight (78,000 ± 500 lux) till 40 min at an interval of 5 min. The intensity of sunlight was measured with portable Lux meter (HI97500 Hanna Instruments, USA). This colloidal solution was checked for the presence of AgNps.

2.8 Characterization of AgNps:

The AgNps synthesized were characterized by UV–vis spectroscopy by scanning in the range of 200–700 nm, at a resolution of 1 nm (ND 1000, Nanodrop Technologies, USA). ATR-FTIR spectroscopy was done using spectrometer having zinc selenide as an internal reflection element to run liquid samples for structure elucidation (Spectrum Two with Pike Miracle^{TM} , Perkin-Elmer). The base line was corrected with water and then 20 µl each of PVD, PVD-$AgNO_3$ and PVD-AgNps were recorded at a resolution of 4 cm^{-1} at the range of 400–4000 cm^{-1}. XRD analysis was performed on a Brucker D8 Advance spectrometer (Brucker, Germany). A thin film of AgNps was deposited on a glass slide. The diffracted intensities were measured from 20^{0} to 80^{0} in 2θ angles, operating at 40 kV and a current of 30 mA with CuK1 radiation (λ = 1.5406 Å) at a 0.045-deg/Min continuous speed. The shape and size of AgNps were determined by a field emission scanning electron microscope (S4800 Type II, Hitachi, Tokyo, Japan) by making a film on glass slide of colloidal AgNps solution on a

double-sided adhesive carbon tape and dried at room temperature. The presence of elemental silver in the sample was determined by energy dispersive spectroscopy (EDAX) (X-Flash detector 5030, Germany). Transmission electron microscopy (FEG-TEM; JEM-2100F, Jeol, Japan, Resolution 0.19nm, 200kV) was used to study further shape and size by applying AgNps on copper grid with operating voltage 200kV with resolution of 0.19 nm. The size of AgNps and percentage distribution of nanoparticles were analyzed by a particle size distribution system (NanoZS-9, Malvern Instruments, UK).

2.9 Antibacterial assay:

The antibacterial activity of the AgNps was scrutinized by the standard Kirby–Bauer disc diffusion method against human pathogenic strains, *Bacillus spizizenii (*ATCC 6633*), Staphylococcus aureus* (ATCC 6538*), Escherichia coli* (ATCC 8739) and *Salmonella typhi* (NCIM 2501). The cell densities of each inoculums were adjusted in culture medium with 0.5 McFarland standards, which was swabbed on the Mueller Hinton agar (MHA) plates using sterile cotton swab. Sterilized paper discs (6 mm diameter) were placed on the MHA plates and then the resultant colloidal solution of AgNps (5 to 20 µl) were loaded on each disc. At the centre of plate, the disc was loaded with 20 µl of purified PVD as a control. The plates were incubated at 37 ^{0}C for 24 h. After the incubation period, the zone of inhibition was determined by measuring the diameter of the zone using (Hi Media, Mumbai) antibiotic zone scale.

3. Results and Discussion:

3.1. Isolation, screening and identification of bacterial strain:

After incubation at 28 ^{0}C for 24 h, colonies developed were screened for fluorescence under UV light when grown on King's B medium which is a characteristic feature of *Pseudomonas*

sp. (See Supplementary Fig. S1). These cultures were screened further for their ability to synthesize siderophores by growing them in 3 different media; SCM, PPM and KMB. Out of 26 isolates, 09 cultures were showing growth with pigmented broth in nearly all media when compared with control. In the culture supernatant, addition to CAS reagent with equal quantities changed its colour from blue to orange, which was indicative of presence of siderophore. Among these cultures, 06 isolates exhibited their ability to synthesize siderophores when grown in all 3 different media. Cell free supernatant exhibited absorbance at 404 nm (See Supplementary Fig. S2) which confirmed the siderophore to be pyoverdin. Further, the positive results with Csaky's and Arnow's assays (absorbance maxima at 525 and 510 nm, respectively) illustrated the presence of mixed (hydroxamate and catecholate) type of siderophores. The isolate SBC-I showed the highest % decolouration of CAS reagent (80%) in succinic acid medium (See Supplementary Table S1) than other media. Hence, it was selected and used for synthesis of siderophores for the further studies. On the basis of morphological and biochemical characterization, the isolate was identified as *Pseudomonas* sp. (See Supplementary Fig. S3) and confirmed by 16S rRNA gene sequencing. The sequence of the total 1409bp (See Supplementary Fig. S4) is available in the GenBank (NCBI) bearing accession No. KJ857033. The evolutionary relationship showed nearest neighbour as *Pseudomonas aeruginosa* with 99% similarity (Fig.1) and hence, SBC-I was named as *Pseudomonas aeruginosa* PSR 213.

3.2 Fermentative production, purification and characterization of siderophore:

After 48 h of incubation, fluorescent green pigment was observed in iron free succinate medium which suggested the synthesis of siderophores. The UV –Vis scan showed two main absorption bands at 232 and 400 nm in UV and visible region which is a characteristic feature of PVD. The XAD purified fractions showed two peaks at 365 nm and 380 nm. After the chromatographic separation on sephadex and BioGel P2, the CAS positive fractions of

siderophore showed absorption maxima in between 400-405 nm which upon HPLC exhibited a sharp single peak at 2.5 min which was similar to the standard PVD (See Supplementary Fig. S5.). Purified PVD was then analyzed using ATR-FTIR for the presence of functional groups in siderophore and the spectrum of absorption bands is shown in Fig. 4A. Band assignments in isolated siderophore explained the presence of i) amino ($-NH_2$) group asymmetric stretching and hydroxyl group (-OH) stretching at 3520 and 3064 cm^{-1} respectively ii) C = O stretching vibrations band at 1564cm^{-1}. The siderophore obtained was PVD having high purity near to homogeneity.

3.3 UV-Vis spectrophotometric titration of $AgNO_3$ with PVD:

Metal free PVD was distinguished by its yellow-green colour. The reported UV-Vis absorption spectrum of PVD from *Pseudomonas aeruginosa* PSR 213 showed major peaks at 230 nm and 400 nm as reported earlier by Meyer and Abdallah [19], where the absorption band at 400nm could be due to the presence of chromophore group [20]. The coordination of Ag^+ with PVD was determined by incremental addition of Ag^+ to PVD solution for which the spectral changes at 400 nm were observed at 0.1 to 1 molar ratio of Ag^+ to PVD. The increase in absorption at 400 nm was observed (Fig. 2a) possibly because of charge transfer from chromophore to Ag^+. Further, gradual addition of Ag^+ did not show any increase in absorbance suggesting the end point of titration with equimolar binding of Ag^+ and PVD (Fig. 2b). This indicated the stoichiometry of Ag^+ and PVD to be 1:1 similar to iron [19].

3.4 Synthesis and Characterization of AgNps:

When an equimolar solution of $AgNO_3$ and PVD was exposed to sunlight, it changed the color from yellow to brown immediately (Supplementary Fig. S7). The shifting from yellow to brown color appears due to the surface plasmon resonance phenomenon (SPR) of AgNps. But, PVD could not synthesize nanoparticles of iron and copper based on its SPR. The

production of the AgNps synthesized from the PVD was evaluated through spectrophotometry in the range of 400–700 nm in a time bound exposure from 0 to 40 min. The absorbance peak was found at 460 nm which increased as a function of reaction time and was the highest at 30 min (Fig.3). After this period of 30 min, the AgNps solution was found to have no significant change in the shift which suggested that there was less variation in its average size. This typical peak at 460 nm confirms the formation of the AgNps [21]. These similar characteristic peaks of the AgNps were observed while preparing AgNps using aqueous leaf extract of *Iresine herbstii*. Broadened band at 460 nm was indication of polydispersed AgNps [22].

The functional groups of PVD involved in binding and reduction of Ag^+ were investigated (Fig.4 A, B and C). Metal free PVD bearing a narrow band of -OH stretching at 3064 cm^{-1} which broadened at 3180 cm^{-1} possibly due to binding of Ag^+ to PVD. The PVD-$AgNO_3$ complex exhibited new peaks at 2918, 2333, 1972 and 1740 cm^{-1} due to changes occurred in confirmation of the PVD. This complex when irradiated with sunlight, it resulted in shifting of band of 3180 to strong stretching of 3305 cm^{-1} which suggested the involvement of hydroxyl groups in the reduction of Ag^+ ions.

The crystalline nature of synthesized AgNps showed (Fig.5) four different peaks having 2θ (degree) at 37.2, 43.7, 65.2 and 77.2. These observed lattice plane value was indexed h, k, l having value of 111, 200, 220 and 311 planes of face centered cubic (FCC) silver, which matched the reported values of International Centre for Diffraction Data (ICDD) card number 03-065-8428. The acute unassigned peak having 2θ (degree) value of especially 30.7 is associated with cubic silicon oxide (cristobalite) with ICDD card number 00-002-0278, since the film was prepared on glass slide.

The synthesized AgNps were analyzed for topographic features and the elements present using FE-SEM coupled with energy dispersive X-ray analysis (EDAX). AgNps were predominantly found to be spherical in shape Fig.6A, but the size of AgNps was difficult to access because resolution of microscope was unsatisfactory. However, the characteristic bright spheres were seen and the elemental analysis for the resultant AgNps was confirmed by EDAX. Signal of Ag peak was observed and designated the presence of AgNps (Fig.6B).

TEM images precisely showed that the AgNps were spherical in shape with size (Fig.6C and 6D) which is close to the size determined by particle size analyzer. The Fig.6E shows the selected area electron diffraction (SAED) pattern of the AgNps. The ring-like diffraction pattern indicated crystalline nature of particles having polydispersity. These concentric diffraction rings appearing as bright spots correspond to the presence of (111), (200), (220), and (311) lattice planes of FCC silver which are also supported by XRD analysis. The calculations suggested that the, d-spacing of 0.428 nm corresponded to the (111) plane of silver. The resultant AgNps formed upon sunlight exposure were examined as a function of time where subsequent reduction in the size of AgNps was observed (See Supplementary Fig. S9). The Fig. 6F shows the particle size distribution of synthesized AgNps between of 6 to 12 nm after 30 min of sunlight exposure.

The biosynthesized AgNps showed antimicrobial activity against human pathogenic bacteria of Gram positive and Gram negative nature by disc diffusion method. The diameter of the zone of inhibition in mm around each different concentration of AgNps solution loaded on paper disc was determined (See Supplementary Fig. S8). A potent pathogen and Gram negative bacterium *Salmonella typhi* showed maximum 17 mm zone of inhibition (See Supplementary Table S2) which may be due to thin cell wall while Gram positive bacteria possess rigid cell wall structure bearing peptidoglycan which might be posing difficulty in penetration of the AgNps [23]. The penetration of AgNps in Gram negative bacteria might

have created pores on the cell membrane leading to death of the cell. Earlier, Sondi and Salopek-Sondi have reported that nanoparticles accumulate on surface of cell wall and forms holes [24] causing cell death.

3.5 Proposed Mechanism of AgNps synthesis:

The silver ions binding to PVD was examined under absence of sunlight using UV-Vis spectrophotometry. PVD has three bidentate metal-binding functional groups which facilitates the binding of the metal cations. Functional groups especially negatively charged hydroxyls and ketones of PVD are involved in binding of Ag^{+}. Moreover, pH plays a major role in coordination of binding of the metal ions with PVD specifically at neutral pH [25]. By considering this fact, the neutral pH was selected while synthesizing the AgNps. The photoreduction of metal umpired by ligands involved ligand-to-metal charge transfer (LMCT) superoxides as a reactive transient [26]. In another example, under the influence of sunlight; dissolved oxygen was responsible to produce superoxides by reacting with phenolic group of humic acid converting Ag^{+} to AgNps [27]. Moreover, photolytic LMCT of metal-siderophore complex leading to decarboxylation-oxidation of siderophore and subsequent reduction of Fe^{3+} ions to Fe^{2+} ions [28]. In this investigation, PVD was utilized for AgNps synthesis, when it gets complexed with Ag^{+} ions, chromophore (hydroxyl groups of phenols) of PVD helped to generate superoxide free radical (O_2^{-}) from dissolved oxygen under photolytic activity and leading to reduction of the monovalent Ag^{+} ions to Ag^{0}. To prove this, we have taken the equimolar mixture of PVD and $AgNO_3$ incubated under two different conditions to create oxygen deficiency (i) continuous purging with 99% pure N_2 gas and (ii) with superoxide dismutase (SOD) in other mixture and exposed to sunlight for 30 min. These results showed that there was no development of SPR of AgNps (see Supplementary Fig. S6). In addition to this, the LMCT plays a major role in further reduction of Ag^{+} ions to AgNps. Primary role of siderophores in the biogeochemical cycle is related to bioavailability of Fe by

its dissolution from minerals which are usually found in marine, fresh water and soils at nanomolar concentrations [29, 30, 31, and 32] while in rhizosphere; it is in high concentration [33] due to elevated plant microbes interaction. Very recently, a review stated the biogeochemical cycle of silver [34] which clearly stated that silver metal is not included in biogeochemical cycles on the earth. The large scale distribution of heavy elements (e.g. Cd, Cu, Hg, Pb) and its isotopes in the marine environment has been investigated thoroughly [35]. The sources of AgNps in the marine environment are mainly through anthropogenic activities as a pollutant. On the other side, Some of the reports are focused on the natural sources of AgNps where the responsible reducing agents for its formation are natural organic matters [36, 37]. Besides this, solar radiations are pertinent to the surface water which can step up the synthesis of AgNps from Ag^{+} in river water, lake water and even marine environment [38] where potent siderophore producing organisms like Pseudomonads are frequently found. In these studies, we have suggested a possible mechanism of AgNps synthesis in the aqueous conditions that supports one of the reasons for synthesis and presence of AgNps traces found in the environment [39].

Conclusion:

Pyoverdin; a well known siderophore of Psuedomonas sp. was explored for the synthesis of silver nanoparticles. An efficient and rapid green method based on the photo induction by means of natural sunlight using siderophore has been established. The polydispersity, (>20nm size) and spherical shapes were the remarkable features in the extracellular siderophore mediated AgNps synthesis. This study opens a new edge in the metal-siderophore interactions and opens avenues to study synthesis of other metal nanoparticles.

Acknowledgment:

All the authors acknowledge the Infrastructural grant through UGC-SAP-DRS (III) (University Grants Commission, New Delhi) & DST-FIST (Dept. of Science & Tech., New Delhi) Govt. of India to School of Life Sciences of this North Maharashtra University. PRD acknowledges the financial support through RFSMS fellowship and from University Grant Commission (UGC), New Delhi.

References:

1. C. Lankford, *CRC Crit. Rev. Microbiol.*, 1973, 2, 273–331.
2. L. Königsberger, E. Königsberger, P. May and G. Hefter, *J. Inorg. Biochem*., 2000, 78, 175–184.
3. H. Boukhalfa and A. Crumbliss, *BioMetals*., 2002, 15(4),325–339.
4. J. Meyer, V. Geoffroy, N. Baida, L. Gardan, D. Izard, P. Lemanceau, and N. Palleroni, *Appl. Environ. Microbiol.*, 2002, 68(6), 2745-2753.
5. I. Lamont, A. Konings, and D. Reid, *BioMetals.*, 2009, 22(1), 53-60.
6. A. Braud, F. Hoegy, K. Jezequel, T. Lebeau and I. Schalk, *Environ. Microbiol.*, 2009, 11(5), 1079-1091.
7. M. Husseiny, M. El-Aziz, Y. Badr and M. Mahmoud, *Spectrochim. Acta, Part A.*, 2007, 67(3), 1003-1006.
8. C. Kumar, S. Mamidyala, B. Das, B. Sridhar, G. Devi and M. Karuna, *J. Microbiol. Biotechnol.*, 2010, 20, 1061-1068.
9. *US Pat*., 12/776,425, 2010.
10. J. Xin, D. Cheng, L. Zhang, K. Lin, H. Fan, Y. Wang and C. Xia , *Int. J. Mol. Sci.*, 2013, 14(11), 21676-21688.
11. L. Arnow, 1937, *J. Biol. Chem.,* 118, 531.
12. A. Gillam, A. Lewis and R. Anderson, 1981, *Anal. Chem. (Washington, DC, US*), 53, 841-844.

13. B. Schwyn and J. Neilands, *Anal Biochem.*, 1987, 160, 47-56.

14. S. Payne, in *Methods In Enzymology.,* ed. S. Colowick and N. Kaplan, New York, Academic Press, USA, 235, 1994, Detection, Isolation, and Characterization of Siderophores, 329-344.

15. N. Saitou and M. Nei, 1987, *Mol. Biol., Evol.,* (4)4, 406-425.

16. J. Felsenstein, *Evolution.*, 1985, 39, 783-791

17. M. Kimura, *J. Mol. Evol.*, 1980, 16(2), 111-120.

18. K. Tamura, G. Stecher, D. Peterson, A. Filipski and S. Kumar, *Mol. Biol. Evol.*, 2013, 30, 2725-2729.

19. J. Meyer and M. Abdallah, *J. Gen. Microbiol.*, 1978, 107, 319-328.

20. S. Philson and M. Llinas, *J. Biol. Chem.*, 1982, 257**,** 8086-8090.

21. D. Notriawan, E. Angasa, T. Suharto, J. Hendri and Y. Nishina, 2013, *Mater. Lett.*, 97, 181-183.

22. C. Dipankar and S. Murugan, *Colloids Surf., B.*, 2012, 98, 112-119.

23. S. Shrivastava, T. Bera, A. Roy, G. Singh, P. Ramachandrarao and D. Dash, *Nanotechnology*., 2007, 18, 225103.

24. I. Sondi and B. Salopek-Sondi, *J. Colloid Interface Sci.*., 2004, 275, 177-182.

25. H. Boukhalfa, S. Reilly, R. Michalczyk, S. Iyer and M. Neu, *Inorg. Chem*., 2006, 45 (14), 5607-5616.

26. A. Rose and T. Waite, *Geochim. Cosmochim. Acta.*, 2006, 70, 3869-3882.

27. M. Gaberell, Y. Chin, S. Hug and B. Sulzberger, *Environ. Sci Technol.*, 2003, 37(19), 4403-4409.

28. K. Barbeau, G. Zhang, D. Live and A. Butler, J. Am. Chem. Soc., 2003, 124 (3), 378-379.

29. P. Mucha, P. Rekowshi, A. Kosakowska A and G. Kupryszewski, *J. Chromatogr. A.*, 1999, 830 (1), 183–189.

30. O. Duckworth, S. Holmström, J. Peña and G. Sposito, *Chem Geol*., 2009, 260(3), 149-158.

31. S. Holmström, U. Lundström, R. Finlay and P. Van Hees, *Biogeochemistry,* 2004, 71(2), 247– 258.

32. S. Essén, D. Bylund, S. Holmström and U. Lundström, *BioMetals*., 2006, 19(3), 269-282.

33. D. Crowley, in *Iron nutrition in plants and rhizospheric microorganisms.*, eds. L. Barton and J. Abadia, Springer, Netherland, 1, 2006, Microbial Siderophores in the Plant Rhizosphere, 169-198.

34. C. Gallon and A. Flegal, *Rev. Environ. Contam. Toxicol.*2015, 235, 27-48.

35. The Lamont Doherty Earth Observatory Columbia University, https://www.ldeo.columbia.edu/res/pi/geotraces/documents/indexDOC/GEOTRACES SciencePlan.pdf, (August 2015).

36. D. Sal'nikov, A. Pogorelova, S. Makarov and I. Vashurina, *Russ. J. Appl. Chem*., 2009, 82(4), 545–548.

37. N. Akaighe, R. MacCuspie, D. Navarro, D. Aga, S. Banerjee, M. Sohn and V. Sharma, *Environ. Sci. Technol.,* 2011, 45(9), 3895–3901.

38. J. Jiang and A. Kappler, *Environ. Sci. Technol.*, 2008, 42(10), 3563–3569.

39. A. Manwar, S. Khandelwal, B. Chaudhari, J. Meyer and S. Chincholkar, *Appl Biochem Biotechnol.*, 2004, 118(1-3), 243-51.

Figure captions:

Figure 1. Neighbor-joining phylogenetic tree of isolated *P.aeruginosa* PSR 213 and it's closely relatives derived from NCBI GenBank Library based on 16 s rRNA gene analysis.

Figure 2a. UV-Vis spectrophotometric titration of Ag^{+} to pyoverdin (PVD) with the gradual addition.

Figure 2b. Molar ratio plot of [Ag^{+} /PVD] to absorbance at 405nm.

Figure 3. UV-Vis spectra of AgNps synthesized as a function of time upon exposure to natural sunlight from 0 to 40 min.

Figure 4. ATR-FTIR spectra of A. Purified PVD, B. PVD-$AgNO_3$ and C. PVD-AgNps.

Figure 5. X-ray diffraction (XRD) spectrum of silver nanoparticles prepared using PVD produced by *Pseudomonas aeruginosa* PSR 213 under natural sunlight.

Figure 6. AgNps characterization by A. Scanning electron microscopy (SEM) at 200nm scale. B. Energy dispersive X-ray analysis (EDAX). C. Fourier transform transmission electron microscopy (FT-TEM) at 50nm scale. D. FT- TEM at 20nm scale. E. Selected area electron diffraction (SAED) pattern. F. Particle size analysis.

Fig. 1

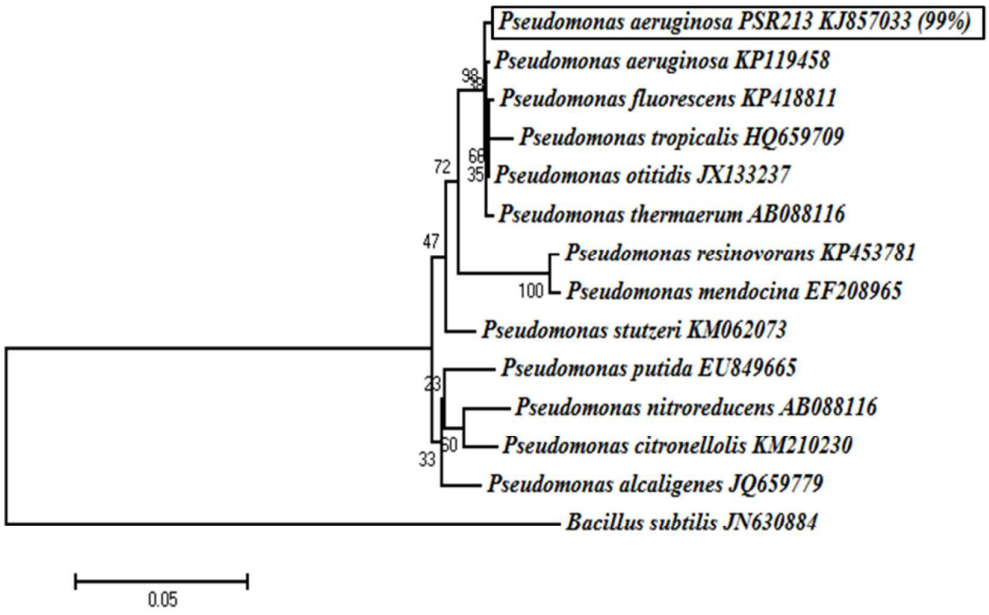

Fig. 2a

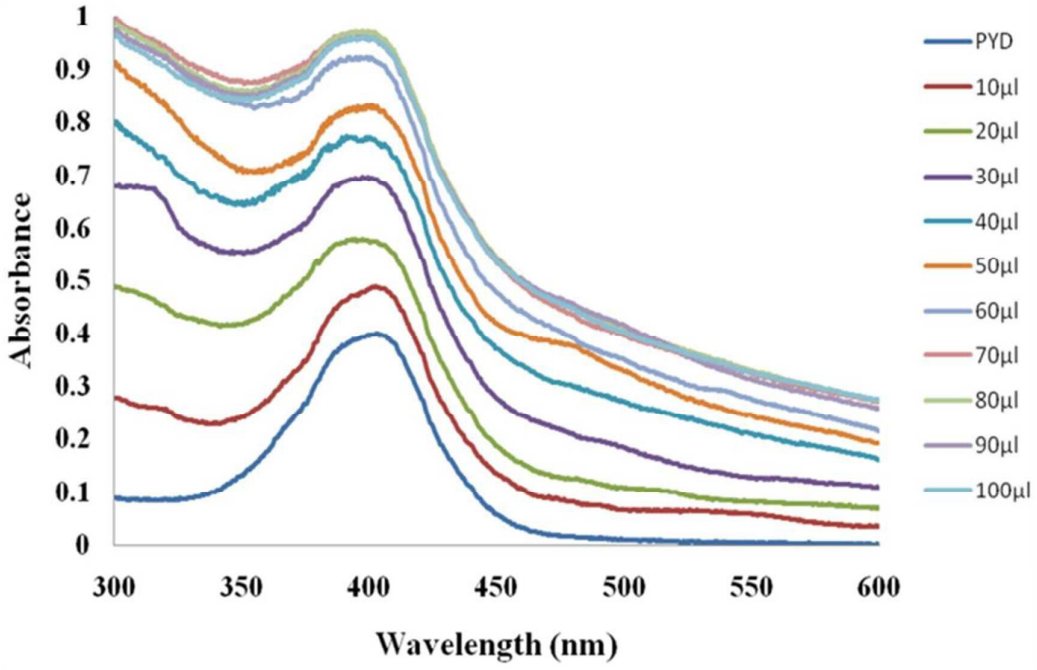

b

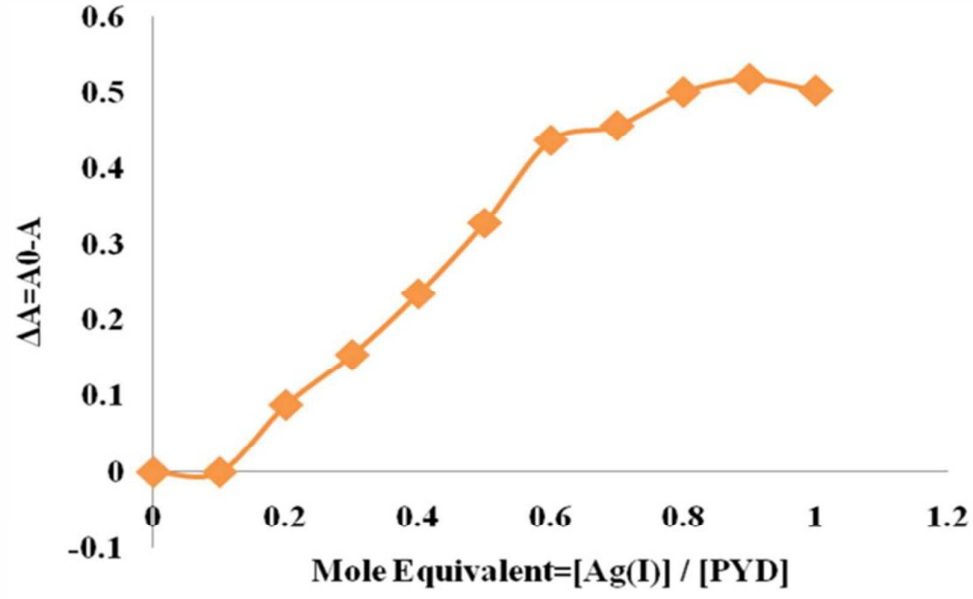

Fig. 3

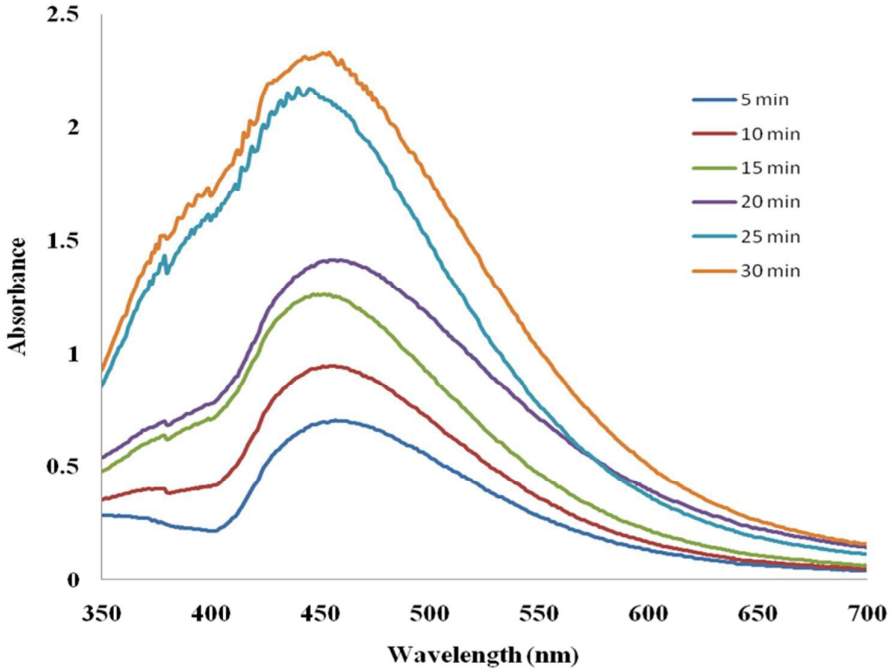

Fig. 4

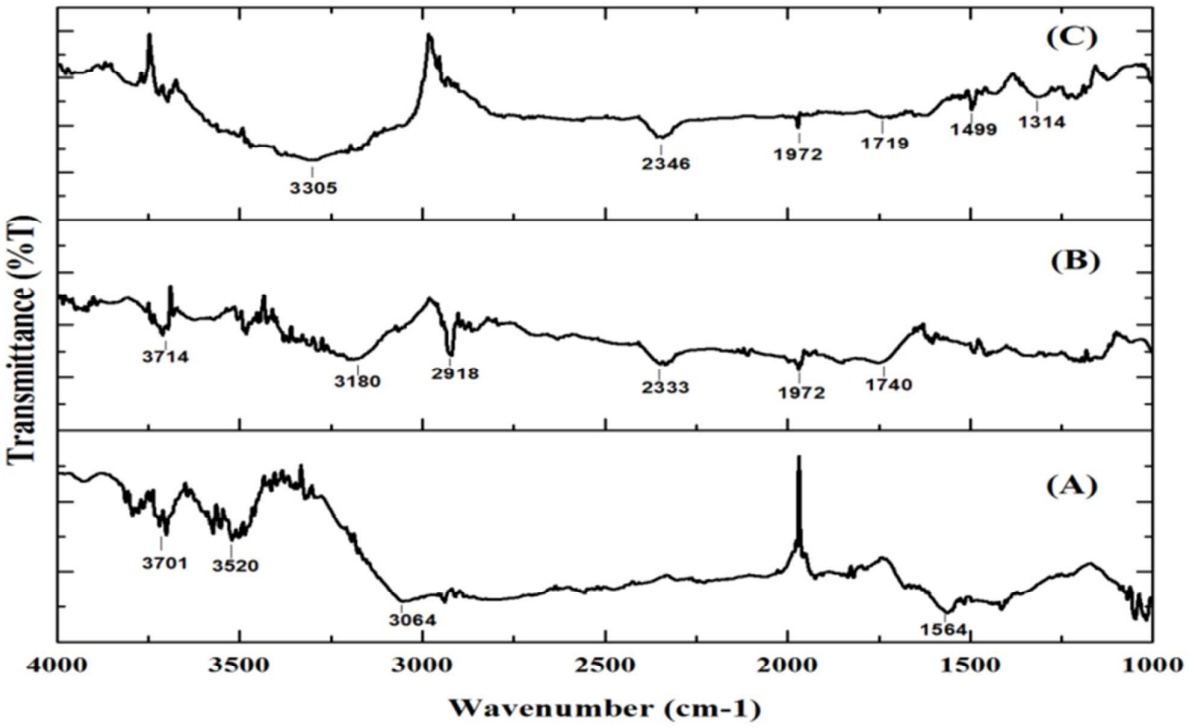

Fig. 5

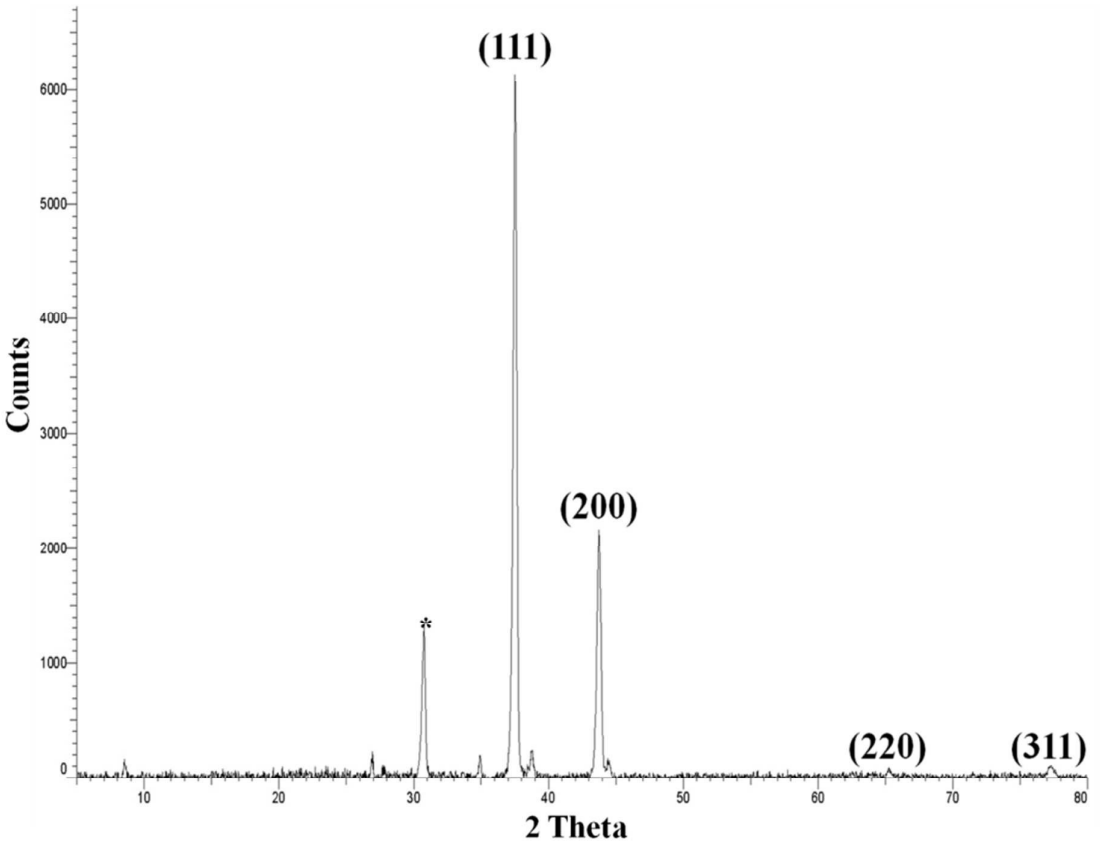

Fig. 6

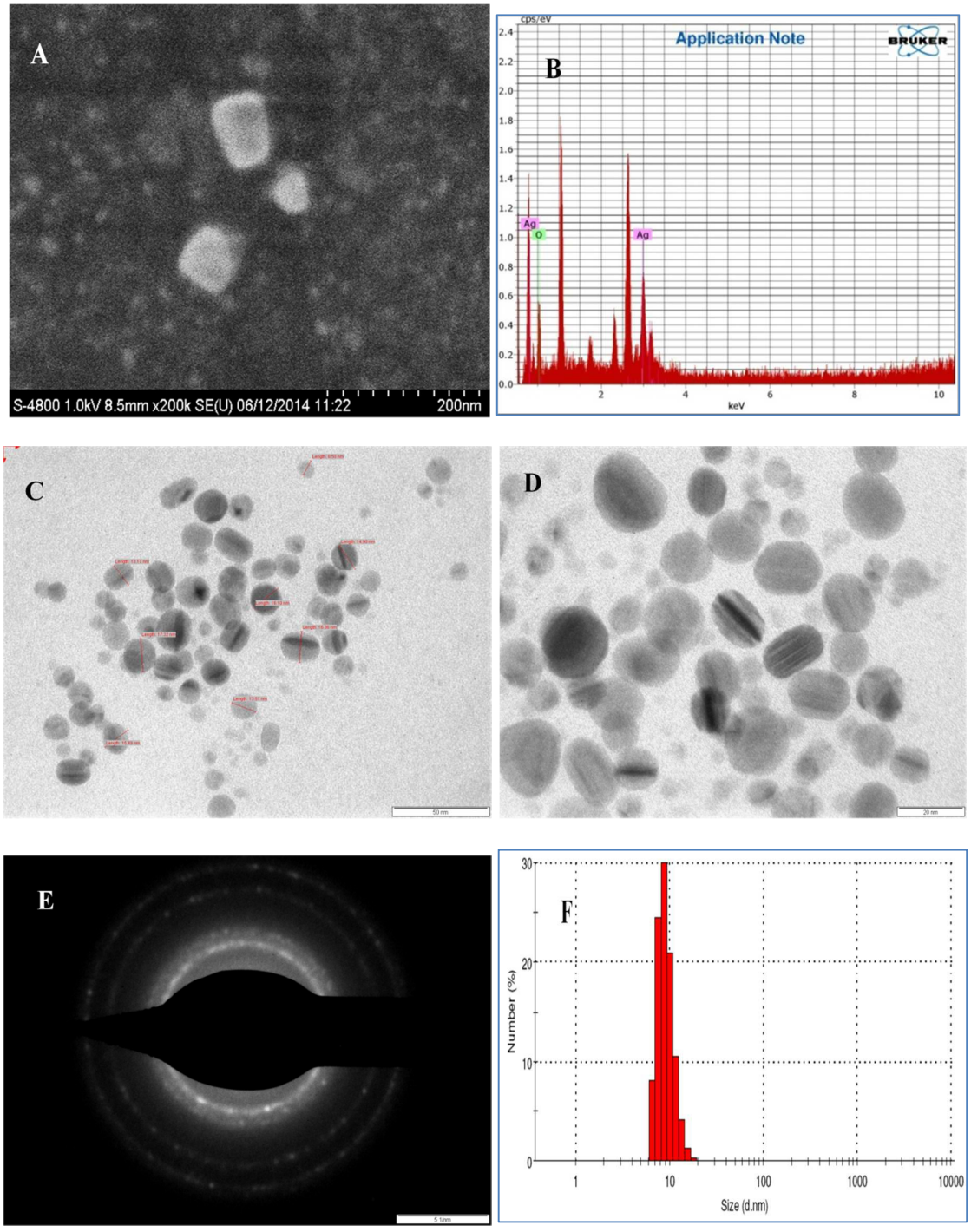

Graphical Abstract: